



Generation of mantle-derived basaltic andesites in volcanic arcs

Elena Melekhova^{*}, Jon Blundy

Department of Earth Sciences, University of Oxford, South Parks Road, OX1 3AN, United Kingdom

ARTICLE INFO

Dr. J. Badro

Key words:

Primary arc magmas
Basaltic andesite
Experimental petrology
Multiple saturation point
Mantle melting
Kamchatka

ABSTRACT

Primary magmas in volcanic arcs exhibit wide compositional diversity on both local and global scales. Processes responsible for this diversity are generally ascribed to some combination of mantle melting or crustal differentiation processes. One widespread view is that arc magmagenesis is driven by combination of H₂O-fluxed and decompression melting of peridotitic mantle wedge, and that primary, mantle-derived melts are high-MgO basalt. However, a variety of other mantle-derived primitive arc magmas, ranging in composition from high-Mg andesite to picrite, has been recognised and it remains unclear to what extent this diversity can be generated by mantle melting processes modulated, for example, by changes in the thermal state of the mantle wedge or the supply of fluid from the slab. Here we use high pressure and temperature experiments to constrain magma generation conditions of a primitive magnesian (8.8 wt% MgO) basaltic andesite from Klyuchevskoy volcano, Kamchatka arc, Russia. We use an inverse experimental approach to define a multiple saturation point on the liquidus surface of the basaltic andesite. The experimental multiple saturation point defines the pressure and temperature at which an erupted melt could have last been in equilibrium with a polymineralic source rock, such as mantle peridotite, and hence provides a robust estimate of magma source conditions.

Equilibrium piston-cylinder experiments were carried out between 0.5 and 1.0 GPa under hydrous conditions (3 to 6 wt% added H₂O) at $f_{O_2} = \Delta NNO+1$. We show that Klyuchevskoy basaltic andesite is multiply saturated with the lherzolite assemblage olivine (Fo₉₀) + clinopyroxene + orthopyroxene + Cr-spinel close to its liquidus ($\geq 95\%$ melt) in the pressure range of 0.6 to 1 GPa (23 to 36 km depth) and 1220–1240 °C. Amphibole is present at temperatures just below the multiple saturation point (≤ 1200 °C). Our results show that basaltic andesite was produced by 8 to 11 wt% partial melting of amphibole-lherzolite source and therefore represents a primary, undifferentiated magma extracted from its source at near-Moho depths. These findings are in a good agreement with geophysical studies of Klyuchevskoy volcano that show magmas are supplied directly from a reservoir at near-Moho depths (25–30 km) through a sub-vertical, pipe-like feeder system. Coeval high-MgO basalts from the volcano may correspond to higher degree mantle melts extracted at slightly greater depths.

Our results provide a tight constraint on the thermal structure of the mantle wedge beneath Klyuchevskoy. Experimental temperatures are higher than those calculated from steady-state thermal models suggesting that upwelling asthenosphere might directly impinge the Moho in a similar fashion to mid-ocean ridges. Intra-arc rifting promotes asthenospheric decompression beneath the Central Kamchatka Depression. The presence of amphibole in our experiments at temperatures up to 1200 °C indicates that dehydration melting of amphibole peridotite formed by metasomatism of mantle wedge by slab-derived fluids is the primary magma generating process. Amphibole stability exercises an important control on melting conditions.

Integrating our results with published multiple-saturation experiments we show that Klyuchevskoy basaltic andesite is one of a family of primary arc magmas whose compositions depend on mantle wedge thermal structure and H₂O activity.

1. Introduction

The starting point for subduction zone magmatism is partial melting of mantle wedge peridotite fluxed and metasomatized by H₂O-rich fluids

derived from the subducting slab (e.g. Bouilhol et al., 2009; Beccera-Torres et al., 2020; Bowman and Ducea, 2023). It is generally accepted that most, but not all, primary magmas are basaltic (e.g. Gaetani and Grove, 2003). This simple scenario considers that the melting process is

^{*} Corresponding author.

E-mail address: elena.melekhova@earth.ox.ac.uk (E. Melekhova).

<https://doi.org/10.1016/j.epsl.2024.118791>

Received 13 January 2024; Received in revised form 17 May 2024; Accepted 18 May 2024

Available online 4 June 2024

0012-821X/© 2024 The Author(s). Published by Elsevier B.V. This is an open access article under the CC BY license (<http://creativecommons.org/licenses/by/4.0/>).

primarily a function of the local temperature and the mass fraction of added H₂O (Till et al., 2012; Katz et al., 2022). The worldwide occurrence of primitive arc magmas (Mg# \geq 0.7) with compositions more evolved than basalt, such as basaltic andesites and high-Mg andesites raises additional questions. There are three main models for the generation of such magmas: partial melting of hydrous mantle peridotite (Baker 1994; Hirose, 1997; Gaetani et al., 1998), assimilation and mixing of primitive basaltic and dacitic melts (Straub et al. 2011), and partial melting of subducted ‘mélange’ material (Kelemen et al., 2003; Marschall and Schumacher, 2012).

An enduring challenge to understanding primary magma generation in arcs is constraining temperatures at which mantle melting occurs, the depth at which melts segregate from their source and start to ascend, the style and degree of mantle melting and even the lithology of the mantle wedge. Of particular importance is the balance between flux melting and decompression melting in arc settings (Schmidt and Jagoutz, 2017).

Here we use experimental petrology to explore the origin of primitive basaltic andesite magmas from Klyuchevskoy volcano, Kamchatka arc, Russian Far East. We apply the inverse multiple saturation approach to constrain the pressure-temperature-H₂O conditions at which Klyuchevskoy basaltic andesites were last in equilibrium with a low-variance, polyminerale source rock by mapping the liquidus surface of the basaltic andesite to search for multiple saturation with a plausible source assemblage (e.g. olivine + orthopyroxene + clinopyroxene + spinel). The magma source depth obtained in this way is then used in conjunction with geophysical observations of the Kamchatka arc and chemistry of lavas and mantle xenoliths to propose a possible scenario for direct generation of basaltic andesites from the sub-arc mantle.

1.1. Constraining magma source depths

Constraining the depths from which a magma was sourced is a key challenge in igneous petrology. Several strategies, as summarised by Schmidt & Jagoutz (2017), can be used. Here we focus on experimental petrology and the determination of points of multiple saturation on the liquidus of a magma (Asimow and Longhi, 2004). At the heart of the multiple saturation concept is the idea that, at the point of extraction from its source, a magma is in equilibrium with a polyminerale source rock. This corresponds to coexistence of a low-variance assemblage at the magma’s liquidus, i.e. when melt fraction is at or close to 95%. In the case of primary (mantle-derived) magmas, the source rock is a peridotite comprising olivine, orthopyroxene, clinopyroxene and an aluminous phase (spinel, plagioclase, garnet). Mantle olivine is typically 91 \pm 1 mol % forsterite (Fo_{91 \pm 1}).

The condition of last equilibrium can be obtained experimentally using either a forward or inverse approach. The forward approach is to melt a putative source lithology and establish at what pressure-temperature conditions a magma with the desired composition could be produced. This requires knowing *a priori* the source rock, for example from mantle xenoliths erupted from the same or nearby volcanic fields. Where the source lithology is not well known, the forwards approach may not yield meaningful results if a good match between erupted and experimental liquid compositions cannot be obtained. In the case of melting beneath volcanic arcs, where H₂O plays a key role in melt generation, an added problem is identifying the H₂O content of the protolith and the phase(s) that host H₂O, e.g. amphibole, phlogopite or nominally anhydrous minerals. The inverse approach circumvents these problems by using liquidus multiple saturation to establish the point where an erupted magma was last in equilibrium with a low-variance assemblage at its liquidus. In practise this requires exploring a region of pressure-temperature space using the erupted magma as a starting composition, along with variable amounts of added H₂O, to locate a liquidus multiple saturation point (MSP). Ideally, *f*_{O₂} is also controlled during experiments. This approach relies critically on knowing that an erupted magma has a true melt composition, unmodified by subsequent magma mixing, crustal assimilation or xenocryst entrainment. The

concept is described in some detail by Blundy (2022) for the case of magmas sourced from crustal depths.

Schmidt & Jagoutz (2017) assembled all published multiply saturated experiments on mafic arc magmas available at the time. They concluded that a wide range of mafic arc magmas could plausibly be derived from sub-arc mantle pressures and temperatures with some influence of mantle wedge thermal structure on magma composition. They report approximately 16 individual studies, showing variable degrees of conformity to their definition of multiple saturation. Using a more stringent requirements we have produced an updated and refined version of the Schmidt & Jagoutz (2017) MSP dataset (Table S1). Experiments were only selected where: (i) erupted lava was found to be in equilibrium with four peridotite phases (olivine + orthopyroxene + clinopyroxene + spinel \pm garnet \pm plagioclase); (ii) Fo content of olivine was in the range 89–92; and (iii) melt fraction was $>$ 90 wt%. According to these criteria only 15 true multiply-saturated experiments were identified (Table S1). These experiments can be subdivided based on the major element chemistry of starting composition: high-magnesian andesite, basaltic andesite, basalt, picrite. Multiple saturation conditions range from 1.0 to 2.7 GPa, 1030–1380 °C and added H₂O contents of 0 to 18 wt%. We note that only one experimentally-studied basaltic andesite (Grove et al., 2003; composition A) can be considered truly primary; other basaltic andesites, such as those from Arenal, Costa Rica (Pertermann and Lundstrom, 2006) and Bezmyanny, Kamchatka (Almeev et al. 2013) are too low in Mg#.

1.2. Klyuchevskoy volcano

Klyuchevskoy is highest active stratovolcano (4754 m) of Eurasia and one of the most active arc volcanoes on Earth. It is located within the Central Kamchatka Depression (CKD), lying east of volcanic arc front formed by westwards subduction of the Pacific plate beneath Asia (Fig. 1). CKD is a 200 km wide graben-like structure produced by intra-arc extension. About 12 active volcanoes, ranging in composition from basalt to andesite, lie within the CKD (Portnyagin et al., 2007). Klyuchevskoy magmas vary in composition from high-MgO basalts to basaltic andesite, with the latter predominant (Fig. 2). Klyuchevskoy produces moderate, but frequent, eruptions approximately every 2 to 5 years. The last largest eruptions occurred in 2007, 2013, 2023 with ash columns reaching 12 km elevation (Ozerov et al., 2020, NASA earth observatory).

There is an extensive literature on Klyuchevskoy and surrounding volcanoes making this one of the best studied arc segments worldwide. Petrology and geochemistry are summarised by Kersting & Arculus (1995), Bergal-Kuvikas et al. (2017) and Churikova et al. (2001) and melt inclusion data are reviewed by Mironov & Portnyagin (2015). Geophysical data are equally extensive: precise earthquake hypocentre locations are provided by Fedotov et al. (2010); seismic tomographic images can be found in Koulakov et al. (2017, 2020); magnetotelluric images of crustal and upper mantle electrical conductivity are presented by Belyavskii (2021). Steady-state numerical models of Kamchatka arc thermal structure are provided by Syracuse et al. (2010) and Plank et al. (2009).

2. Experimental approach and analytical methods

We chose as our starting material a high-MgO Klyuchevskoy basaltic andesite with primitive magma characteristics (KLU-96-03, Churikova et al. 2007¹). KLU-96-03 is a mildly porphyritic, vesicular Holocene lava with olivine and augite phenocrysts (\leq 10 vol%) in a groundmass of plagioclase, pigeonite, magnetite, augite and brown glass. Phenocrystic olivine cores are Fo_{90–86} often containing chromite inclusions (Cr# \geq 0.7). Whole-rock Cr and Ni contents are high, 426 and 151 ppm

¹ This sample is referred to as IKLU-03, CKD, Q4 in Churikova et al. (2001)

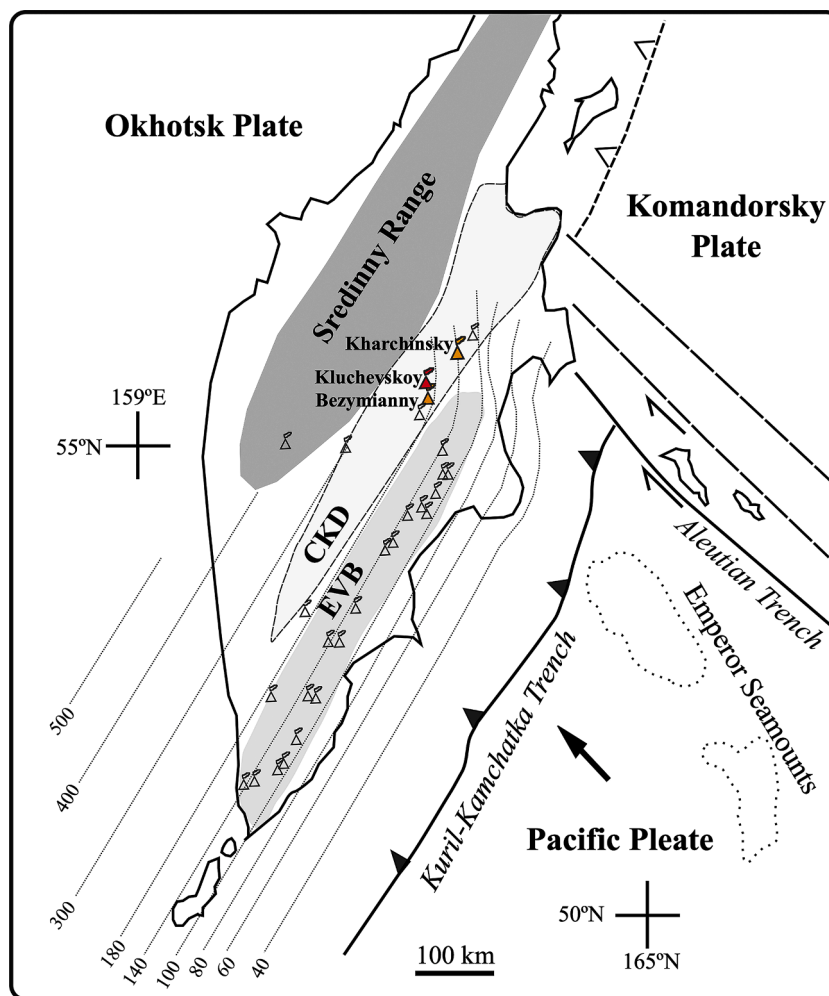


Fig. 1. Plate tectonic map of the Kurile-Kamchatka volcanic arc, showing the location of the Klyuchevskoy (red triangle) and two other volcanoes discussed here (orange triangles). Other Kamchatka volcanoes are shown as non filled triangles. CKD is the Central Kamchatka Depression formed by intra-arc extension.

respectively. $Mg\#$ of bulk rock calculated with all Fe as FeO_{tot} is 66. KLU-96-03 is very similar to high-MgO basalts from the 1932 eruption described by Kersting & Arculus (1994). The estimated eruption temperature of KLU-96-03 is 1270 ± 20 °C (olivine-liquid geothermometer of Putirka et al., 2008) and ~ 1140 °C (for similar basaltic andesites) from two-pyroxene thermometry (Kersting & Arculus, 1993). The fO_2 can be calculated from the FeO/Fe_2O_3 ratio of erupted lavas provided that no post-emplacement or degassing-induced oxidation has occurred. Although Churikova et al. (2001) report only FeO_{tot} , four basaltic andesites from Khubunaya et al. (1994) with very similar compositions to KLU-96-03 have measured Fe_3/Fe_{tot} in the range 0.28 to 0.40. Their calculated fO_2 (at 1220 °C and atmospheric pressure) ranges from $NNO + 2.1$ to $NNO + 1.0$ (mean $\Delta NNO = 1.4 \pm 0.5$). We assume that a similar value would pertain to KLU-96-03 and that this represents a good estimate of the redox state of our starting material. The chosen sample lies close in composition to another primitive basaltic andesite (JR-28) from Jorullo, Mexico, studied experimentally by Weaver et al. (2011). Major element compositions of both starting materials are presented in Table 1 and trace element data for KLU-96-03 in Sup_Table 2. The range of initial H_2O contents (2 to 6 wt%) used in our experiments bracket the range of H_2O contents in olivine-hosted (Fo_{85-90}) melt inclusions from Klyuchevskoy (≤ 5 wt%; Auer et al., 2008; Mironov et al., 2015).

Powdered KLU-96-03 was dried at 200 °C and stored in a box-oven. Annealed $Au_{80}Pd_{20}$ (2 mm OD) capsules were filled with dried starting material and deionised H_2O was added by pipette. Capsules were welded and inserted into an $Au_{80}Pd_{20}$ outer capsule (4 mm OD) which was also

filled with starting material powder and the same amount of deionised H_2O . Experiments were carried out in half-inch (12.7 mm), end-load piston cylinder apparatus with NaCl-Pyrex-MgO assembly at University of Oxford. The assembly was calibrated by NaCl melting (Siewert et al. 1998) and the quartz-coesite transition (McDade et al., 2002); a -3% friction correction was applied. A $We_{95}Re_5/W_{75}Re_{25}$ (Type D) thermocouple with a calibrated accuracy of ± 5 °C was used to monitor temperature; no correction of pressure on thermocouple e.m.f. was applied.

It is difficult to control fO_2 in piston cylinder experiments due to the permeability of hydrogen and carbon through capsule and cell material. Consequently, during each run experimental fO_2 is mediated through redox reactions involving H_2O , CO_2 , FeO and Fe_2O_3 inside the capsule. We do not buffer fO_2 externally. Instead, we use the double-capsule technique whereby an outer capsule filled with the same starting materials serves to delay the ingress or egress of H and C and minimise H_2O loss (Hall et al., 2004; Kägi et al., 2005). In this way we preserve the original Fe^{3+}/Fe^{2+} ratio of the starting materials during the experiment (e.g. Melekhova et al., 2015; Becerra-Torres et al., 2020). To check our experimental method, we estimated the fO_2 for three experiments using Ballhaus et al. (1991) olivine-spinel oxybarometer. Estimated fO_2 ranges from 1.2 to 1.9 log units above the NNO buffer, in very good agreement with calculated fO_2 of natural samples ($\Delta NNO = 1.4 \pm 0.5$).

Major element compositions of experimental phases were analysed by electron microprobe on a Cameca SX-5, FEG instrument at University of Oxford using standard calibration techniques with oxide and silicates.

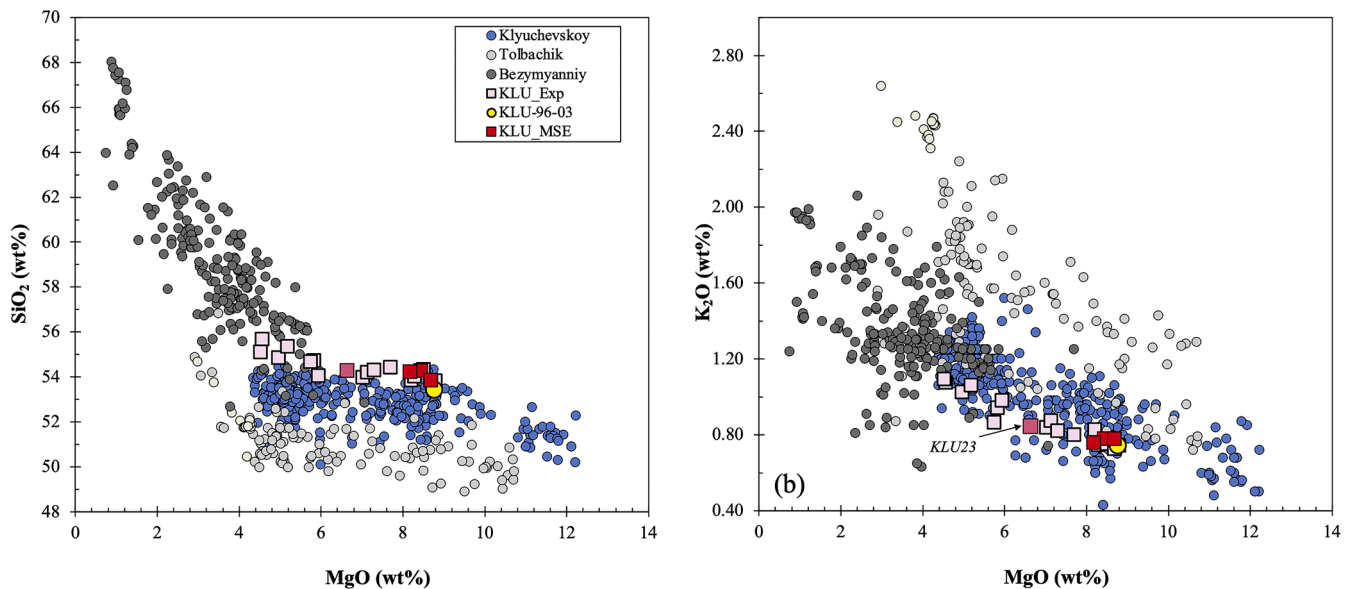


Fig. 2. Whole rock (a) SiO₂ and (b) K₂O variations of Kluchevskoy lavas plotted versus MgO (normalised anhydrous). Starting composition, KLU-96-03, is shown with the yellow circle. Lavas from Tolbachik and Bezmyannyi volcanoes are presented for comparison. Data from GEOROC. Experimental glasses are shown as squares. Red squares denote glasses saturated with a lherzolitic assemblage ($\geq 92\%$ melt) and lie close to KLU-96-03, multiply saturated liquids. Orange square labelled KLU23 is a lherzolite-saturated melt ($< 91\%$ melt) whose composition differs from that of KLU-96-03. By definition multiply saturated experimental liquids have this composition.

Table 1

Experimental starting composition

Starting compositions of basaltic andesite starting materials from this study (KLU-96-03) and from Weaver et al. (2011).

| Oxide | KLU-96-03 | JR-28 |
|--------------------------------|-----------|--------|
| SiO ₂ | 53.70 | 53.16 |
| TiO ₂ | 0.85 | 0.77 |
| Al ₂ O ₃ | 15.33 | 16.18 |
| FeO _{tot} | 8.27 | 7.57 |
| MnO | 0.16 | 0.13 |
| MgO | 8.88 | 9.43 |
| CaO | 9.40 | 8.41 |
| Na ₂ O | 2.89 | 3.42 |
| K ₂ O | 0.76 | 0.79 |
| P ₂ O ₅ | 0.16 | 0.15 |
| Total | 100.40 | 100.01 |
| Ni (ppm) | 151 | 261 |
| Cr (ppm) | 426 | 564 |
| Mg# | 0.66 | 0.69 |

FeO_{tot} - iron total.

KLU-96-03 - basaltic andesite from Klyuchevskoy volcano, Central Kamchatka. Depression (Churikova et al., 2011).

JR-28 - basaltic andesite from Volcán Jorullo, Michoacan-Guanajuato Volcanic Field.

Trans-Mexican Volcanic Belt (Weaver et al., 2011).

Analytical set-up was that of Becerra-Torres et al. (2020). Modal proportions of phases were determined by least-squares regression. Volatile (H₂O, CO₂) contents of experimental glasses were analysed by secondary ion mass spectroscopy (SIMS) at the NERC facility, University of Edinburgh, using a Cameca IMS 7f-Geo instrument with nominal 10 kV primary beam of ¹⁶O⁻ ions, 5 nA beam current, and spot size at the sample surface $\sim 15 \mu\text{m}$. H₂O and CO₂ were calibrated against synthetic basaltic glass standards (Shiskina et al., 2010) containing $\leq 3.5 \text{ wt\%}$ H₂O and $\leq 2000 \text{ ppm}$ CO₂.

3. Results

Experimental run conditions, phase assemblages and phase

proportions are presented in Table 2, along with H₂O and CO₂ content of experimental glasses and H₂O activity ($a_{\text{H}_2\text{O}}$) in the melt calculated using the method of Burnham (1979). Mineral and glass chemistry of run products are reported in Supplementary Material Table 2.

Several factors can affect equilibrium in this kind of experiments: insufficient run duration, temperature gradients, and lost or gain of volatiles. In most of our runs there is no significant difference between added H₂O and that measured by SIMS in run products after allowing for crystallisation of anhydrous minerals. CO₂ contents of experimental glasses are consistent in all but one experiment (KLU20) suggesting that it most likely was present in the starting composition rather than gained during the run by diffusion from the graphite furnace (Gaetani et al., 1998; Stamper et al., 2014; Melekhova et al., 2015). Previous experiments on hydrous basalts demonstrated that run durations of ~ 20 – 24 hours are sufficient to reach equilibrium (e.g. Sisson and Grove, 1993a). Systematic variations in melt compositions, melt fraction and phase proportions with pressure and temperature are suggestive of close approach to equilibrium (Table 2). Mass balance calculations consistently have sum of residuals < 1 . Crystal morphology suggests that there were no nucleation problems (Fig. 3). Crystals are equant, however patchy and concentric zoning in SiO₂, Al₂O₃ and MgO is observed in many pyroxenes (Table S2). This is not unusual in natural rocks or experiments on basalts (e.g. Ubide et al., 2019), and is difficult to eliminate without compromising other aspect of experiments, for example increasing run duration most likely will result in change in volatile content and f_{O_2} .

We present our experimental results for all near-liquidus ($> 91\%$ melt) experiments as a liquidus surface diagram (Fig. 4a). Our experiments are complemented by those of Weaver et al. (2011) at pressures above 1 GPa. Melt composition in experimental run products with melt fraction less than 91% is more evolved than KLU-96-03 and cannot be used to constrain source extraction conditions, although these experiments provide useful indications of other minerals that are stable close to the liquidus. Of the seven near-liquidus runs in Table 2 and Fig. 4a, four (KLU11, 14, 18, 23) bracket a small triangular region of liquids multiply saturated with a lherzolite assemblage (olivine + clinopyroxene + orthopyroxene + Cr-spinel); between 0.6 and 1 GPa and 1220 to 1240 °C, for melt H₂O contents of 3.5 to 5 wt%. This region is bounded

Table 2

Experimental run conditions, phase proportions, melt volatile contents and selected mineral compositions.

| Run number ^a | T °C ^b | P GPa | duration hours | H ₂ O _{initial} wt % added | Run products ^c | ΣR ² | H ₂ O _{melt} SIMS, wt% | CO ₂ melt SIMS, ppm | a (H ₂ O) ^d | ^Δ NNO | Fo mol % | Mg# ^e cpx/opx | Cr# ^f spinel |
|--------------------------|-------------------|-------|----------------|--|---|-----------------|--|--------------------------------|-----------------------------------|------------------|----------|--------------------------|-------------------------|
| KLU12 | 1220 | 1.0 | 24 | 2.0 | gl (81), cpx (14), opx (4), sp (1) | 0.56 | 2.93 (0.18) | 599 (39) | 0.20 | | | 86/88 | – |
| KLU9 | 1260 | 1.0 | 25 | 3.0 | gl (100) | 0.07 | 3.35 (0.01) | 524 (15) | 0.28 | | | | |
| KLU19 | 1220 | 1.0 | 24 | 3.2 | gl (87), cpx (10), opx (3) | 0.58 | 3.60 (0.05) | 716 (22) | 0.27 | | | 86/90 | |
| KLU28 | 1250 | 0.8 | 20 | 3.0 | gl (91), cpx (7), opx (1.4), sp (tr) | 0.34 | 2.57 (0.03) | 483 (40) | 0.21 | | | 84/85 | |
| KLU23 | 1240 | 0.6 | 24 | 3.0 | gl (91), ol (4), cpx (5), opx (tr), sp (tr) | 0.03 | 3.06 (0.11) | 485 (8) | 0.30 | 1.24 | 90 | 88/89 | 47 |
| KLU30 | 1250 | 0.5 | 22 | 3.0 | gl (100) | 0.39 | 2.91 (0.07) | 426 (18) | 0.34 | | | | |
| KLU32^g | 1245 | 0.5 | 23 | 3.0 | gl (98), ol (1), cpx (0.6), sp (tr), mg (tr) | 0.29 | 3.09 (0.06) | 474 (19) | 0.37 | | 92 | 91/- | 20 |
| KLU14 | 1220 | 0.8 | 24 | 4.7 | gl (100), ol (tr), opx (tr), cpx (tr), sp (tr) | 0.11 | 3.91 | 596 | 0.38 | 1.91 | 90 | 90/87 | 47 |
| KLU11 | 1220 | 0.7 | 23 | 4.4 | gl (100), ol (tr), opx (tr), cpx (tr), sp (tr) | 0.15 | 3.87 (0.13) | 537 (24) | 0.41 | | 91 | -/89 | – |
| KLU18 | 1220 | 0.6 | 20 | 4.7 | gl (99), ol (tr), opx (tr), cpx (tr), sp (tr) | 0.05 | 4.10 (0.05) | 417 (54) | 0.46 | 1.17 | 89 | 89/90 | 46 |
| KLU13 | 1210 | 0.8 | 24 | 4.0 | gl (82), cpx (13), opx (5), sp (tr) | 0.11 | 4.39 (0.19) | 556 (37) | 0.37 | | | 89/90 | 49 |
| KLU10 | 1200 | 1.0 | 23 | 3.0 | gl (74), cpx (21), opx (5), plag (tr) | 0.03 | 4.03 (0.40) | 717 (41) | 0.26 | | | 86/86 | |
| KLU8 | 1220 | 1.0 | 26 | 3.0 | gl (72), cpx (21), opx (7), sp (tr) | 0.08 | 3.39 (0.05) | 602 (2) | 0.22 | | | 83/86 | 43 |
| KLU20 | 1230 | 1.0 | 24 | 3.3 | gl (79), cpx (16), opx (5) | 0.18 | 4.3 (0.14) | 1875 (28) | 0.30 | | | 88/88 | |
| KLU21^g | 1200 | 1.0 | 24 | 5.0 | gl (69), cpx (14), opx (3), amph (14), sp (tr), mg (tr) | 0.05 | n.a | n.a | | | | 82/84 | 67 |
| KLU16 | 1220 | 1.0 | 24 | 4.5 | gl (95), cpx (5), opx (tr), sp (tr) | 0.14 | 4.80 (0.14) | 551 (26) | 0.40 | | | 89/90 | 59 |
| KLU3 | 1150 | 1.0 | 6 | 3.9 | gl (69), cpx (20), opx (7), amph (3), mg (tr) | 0.10 | 5.50 (0.50) | 793 | 0.38 | | | 85/83 | |
| KLU17 | 1180 | 1.0 | 24 | 5.0 | gl (87), cpx (10), opx (3), sp (tr) | 0.52 | 6.14 (0.18) | 527 (31) | 0.49 | | | 83/85 | |
| KLU22 | 1210 | 0.9 | 23 | 5.0 | gl (88), opx (2), cpx (9), sp (tr) | 0.57 | 6.02 (0.34) | 482 (41) | 0.52 | | | 88/89 | 42 |
| KLU29 | 1215 | 0.7 | 21 | 6.0 | gl (100), sp (tr) | 0.55 | n.a | n.a | | | | | 52 |
| KLU31 | 1210 | 0.5 | 20 | 6.0 | gl (100) | 0.41 | 5.43 (0.04) | 354 (10) | 0.70 | | | | |

^a Runs in bold are near-liquidus experiments containing 3 or more mineral phases.^b Temperatures in italics indicate fluctuations of ± 40 °C during run.^c By mass balance; tr denotes < 0.5%.^d H₂O activity at experimental P and T calculated using the method of [Burnham \(1979\)](#) and the measured H₂O in glass, assuming Fe³⁺/Fe_{tot} = 0.3;.^e Mg# = molar Mg/(Mg+Fe²⁺)*100, average is reported;.^f Cr# = molar Cr/(Cr+Al+Fe³⁺)*100,^g Runs KLU21 and KLU32 contain two oxide phases; Cr-spinel (sp) and magnetite (mg).^Δ NNO - calculated using [Ballhaus et al., 1991](#) olivine-orthopyroxene-spinel oxygen geobarometer.

at above 1 GPa by the disappearance of clinopyroxene and below ~0.5 GPa by the disappearance of orthopyroxene, thereby providing a pressure interval for lherzolite multiple saturation. The upper temperature stability limit of lherzolite saturation is defined by the pressure-dependent olivine-out curve. Our experiments do not bracket the low temperature stability of lherzolite, however the absence of olivine in two sub-liquidus runs (87–88% melt) with melt H₂O contents of 6 wt% (KLU17 at 1180 °C, 1 GPa) and added H₂O of 5 wt% (KLU22 at 1210 °C, 0.9 GPa) suggest that the low-temperature side of the multiple saturation field is defined by a second, near-isothermal olivine-out curve at ~1210 °C. Experiments that define lherzolite MSPs have Fo_{89–90} olivine with 0.2 wt% MnO. Spinel is chromite with Cr#_{46–49}. Clinopyroxene has Mg#_{87–89} and 2–4 wt% Al₂O₃; orthopyroxene has Mg#_{87–89} and 2.7–3.8 wt% Al₂O₃ (Fig. 5). Melt H₂O contents lie between 3.1 and 4.1 wt%.

Pargasitic amphibole with >13.5 wt% Al₂O₃ is present alongside clinopyroxene, orthopyroxene and spinel (but not olivine) in two 1 GPa sub-liquidus runs: at 1150 °C with 5.5 wt% H₂O in the melt (KLU3) and at 1200 °C with 5 wt% added H₂O (KLU21). These temperatures lie

within 20 °C of the MSPs. They are significantly higher than the upper temperature stability of pargasite in peridotite at high H₂O activities ([Green et al., 2014](#)), but in good agreement with amphibole stability under reduced aH₂O at ≥ 2 GPa ([Juricek and Keppler, 2023](#)). For example, at 2 GPa, [Juricek & Keppler \(2023\)](#) define amphibole-out at 1210 °C at aH₂O = 0.5 rising to 1320 °C at aH₂O = 0.25. For comparison, calculated aH₂O in our MSP melts (3.1 to 4.1 wt% H₂O) is in the range 0.30 to 0.46 (Table 2). Thus, the KLU-96–03 MSP lies very close to the upper stability limit of amphibole in peridotite under conditions of reduced aH₂O (~ 0.4). The absence of experiments with liquidus amphibole suggests that its liquidus field is very small for KLU-96–03 and likely close to 1 GPa.

Plagioclase (An₅₆) is present in a single sub-liquidus run (KLU10) alongside clinopyroxene and orthopyroxene. Coexisting Cr-spinel and aluminous magnetite occur in two runs (KLU21 and KLU32). Phlogopite does not occur in any of our experimental runs reflecting the low K₂O of KLU-96–03.

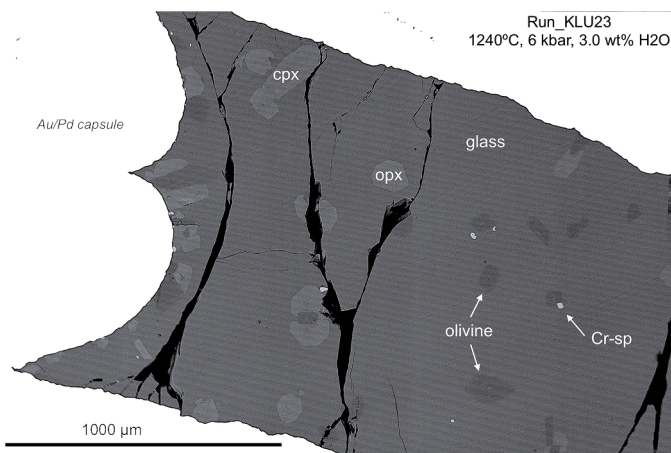


Fig. 3. Back-scattered electron image of typical, near-liquidus experimental run product. Inner Au₈₀/Pd₂₀ capsule of KLU23 showing a homogeneous, multiply-saturated run product with high melt fraction (91%). ol – olivine, cpx – clinopyroxene, opx – orthopyroxene, Cr-sp – chrome-spinel.

4. Discussion

Our experimental results demonstrate that KLU-96-03 can be produced by direct partial melting of lherzolite at 1220 to 1240 °C and pressures between 0.6 and 1.0 GPa at or slightly above the amphibole-out curve. A previous attempt to obtain lherzolite multiple saturation for Jorullo basaltic andesite (Weaver et al., 2011) was unsuccessful because experiments were performed at too high pressures (1 to 2 GPa).

Nonetheless, Weaver et al. (2011) experiments are broadly consistent with those presented here, showing liquidus olivine or orthopyroxene (\pm spinel) without clinopyroxene at pressures ≥ 1 GPa (Fig. 4a).

To test if melt composition in our MSP experiments is consistent with that of KLU-96-03, we plot experimental glass compositions alongside whole rock analyses of Klyuchevskoy lavas (Fig. 2). MSP glasses lie close to KLU-96-03 except for run KLU23, where melt fraction is only 91% compared to 98–100% in the other three MSP experiments. Even though SiO₂ in KLU23 glass matches KLU-96-03, differences in MgO and K₂O (Fig. 2) and other elements (Supplementary Material Table 2) are too large for KLU23 to be considered a true liquidus MSP.

There are several additional sources of information that can be used to corroborate our experimental findings; H₂O content of primitive melt inclusions, calculated eruption temperatures, mantle xenolith and lava mineral assemblages and chemistry, mass balance of experimental results to a mantle source rock, and geophysics.

4.1. Comparison to mineral compositions from lavas and xenoliths

Mineral compositions from experimental run products are compared with phenocrysts from Klyuchevskoy lavas and Kamchatka mantle xenoliths in Fig. 5. Although there are no reported mantle xenoliths from Klyuchevskoy, peridotite xenoliths are reported from nearby Bezymianny and Kharchinsky (Figure 1; Shcherbakov et al., 2011; Ionov et al., 2013; Davydova et al., 2019; Siegrist et al., 2019; Sekisova et al., 2021). A recent geophysical study of magmatic activity of Klyuchevskoy and Bezymianny between 2000 and 2022 (Kiryukhin et al., 2023) suggests that the two volcanoes have a common magmatic source.

Klyuchevskoy high-MgO basalts are characterised by phenocrysts of olivine (cores Fo₉₀₋₈₀) with Cr-spinel inclusions (Cr# ≥ 70),

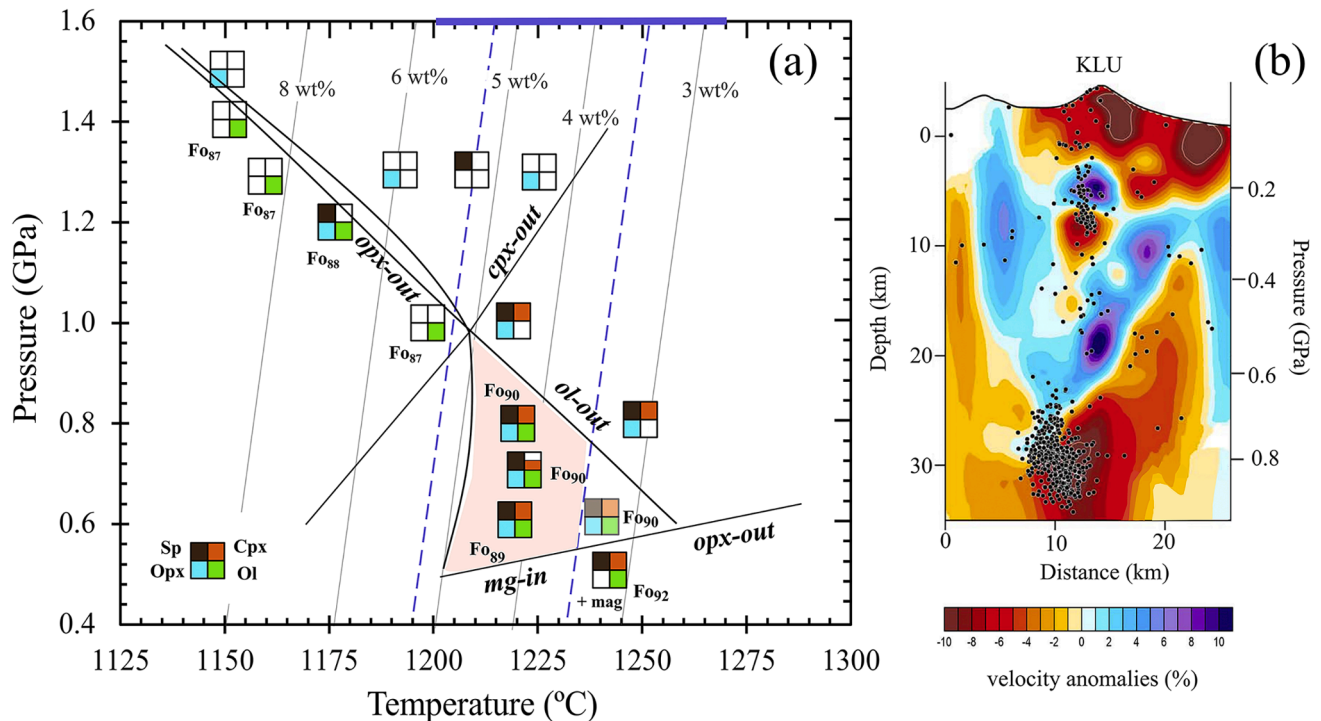


Fig. 4. (a) Liquidus surface diagram for high-MgO basaltic andesite (KLU-96-03) used to define the liquidus multiple saturation point. Only experiments with $\geq 90\%$ glass are plotted. Olivine composition (mole% Fo) shown next to experimental symbols. Liquidus contours (dashed grey lines) are labelled with the corresponding H₂O content of the melt. The pink shaded area is the region of last equilibration of KLU-96-03 with mantle lherzolite. It was defined by two olivine-out and two pyroxene-out curves. The water content range of melt inclusions and eruptive temperature of high-MgO basaltic andesite lavas of Klyuchevskoy volcano are shown by the blue bar and dashed lines respectively. Liquidus experiments on high MgO-basaltic andesite (JR-28; Table 1) from Volcano Jorullo, Mexico (Weaver et al., 2011) at pressures ≥ 1 GPa are plotted to constrain phase stability at high pressures. (b) Tomographic image, adapted from Koulakov et al. (2017), showing S-wave velocity anomalies beneath Klyuchevskoy volcano (KLU). The black dots are earthquakes. Note the agreement between the location of deep earthquakes (22–35 km) and experimentally determined last equilibration of KLU-96-03 with lherzolite (23–36 km; 0.6 to 1 GPa) in (a). The cluster of earthquakes at ~ 9 km depth is attributed to degassing and associated crystallisation.

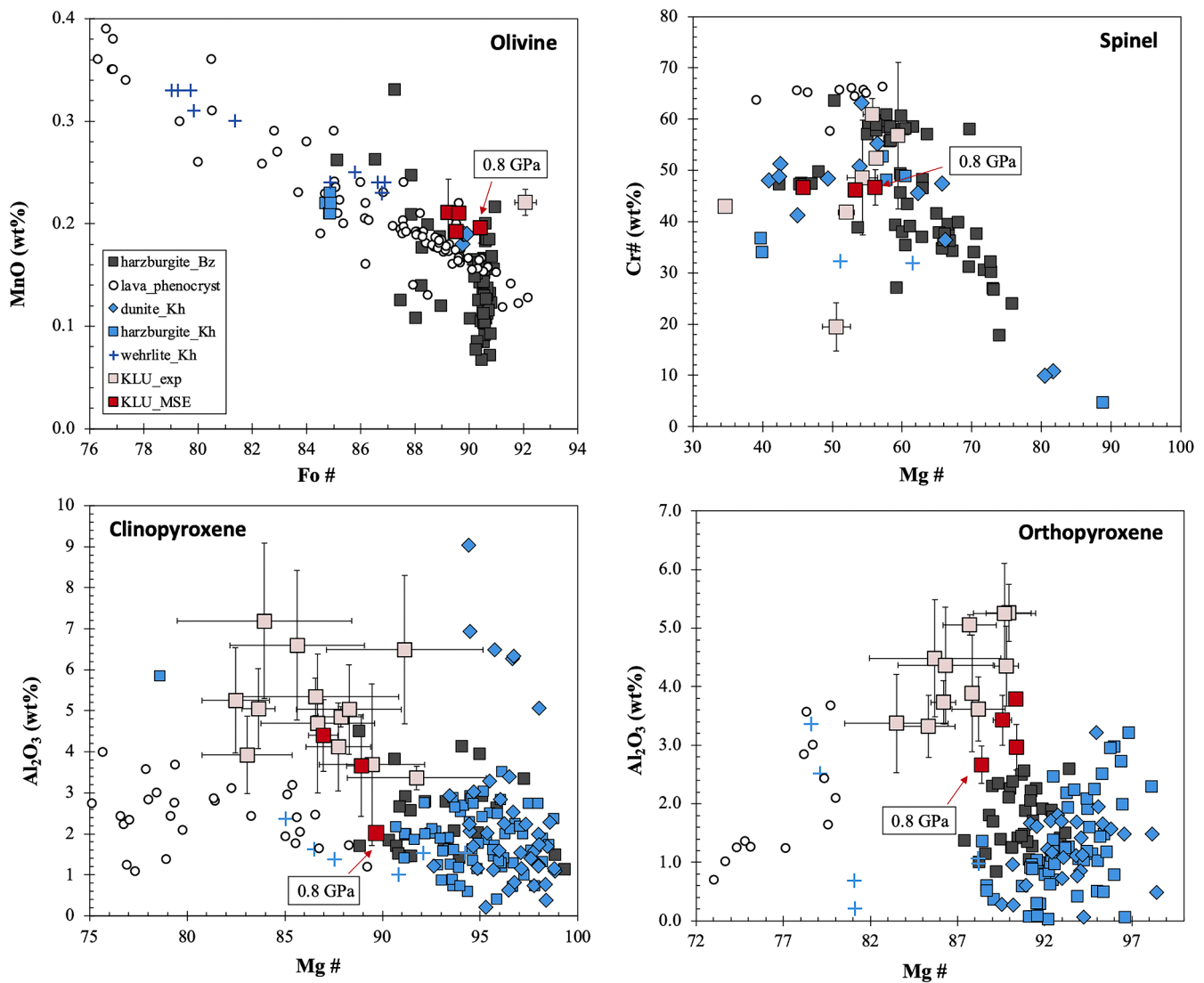


Fig. 5. Compositional variations of olivine (a), spinel (b), clinopyroxene (c) and orthopyroxene (d) for mantle xenoliths from Bezmyianny (Bz) and Kharchinsky (Kh) and phenocrysts from Klyuchevskoy lavas are compared to mineral phases from this experimental study. KLU_MSE – mineral phases from near liquidus multiply-saturated experiments, and KLU_exp – all other experiments. Data are in Supplementary Table 2 and 3. Error bars are 1 s.d. The 0.8 GPa multiply-saturated experiment (KLU14) is indicated.

clinopyroxene (Mg#_{89–75}), and rare orthopyroxene (Mg# < 80). The most magnesian olivines (Fo_{89–90}) have lower MnO compared to experimental olivines (Fig. 5a). Olivine phenocrysts follow a differentiation trend with decreasing Fo and increasing MnO, whereas experimentally-produced MSP olivines cluster around Fo_{89–90} and ~0.2 wt% MnO. Olivine from KLU32, a 0.5 GPa liquidus experiment with only three crystal phases (spinel, olivine, clinopyroxene) has Fo₉₂ with slightly higher MnO. Spinel from lavas has higher Cr# and lower Mg# than any of the experimental spinels (Fig. 5b). Clinopyroxenes (Fig. 5c) and orthopyroxenes (Fig. 5d) from lavas plot at consistently lower Al₂O₃ and Mg# than experiments suggestive of crystallisation at lower pressures from slightly more evolved liquids, as expected for magma crystallisation during ascent.

Ultramafic xenoliths from Bezmyianny and Kharchinsky are characterised by complex textures and mineralogy with a notable presence of amphibole, often as veins or reaction products. Bezmyianny xenoliths comprise coarse spinel harzburgites with orthopyroxene reaction rims against host andesite. Ionov et al. (2013) identify three textural generations in the following sequence: (1) olivine + orthopyroxene + spinel; (2) olivine + orthopyroxene + clinopyroxene + Cr-spinel; (3) olivine + clinopyroxene + amphibole + plagioclase. They attribute this textural

evolution to progressive interaction of mantle harzburgite with melts and fluids producing amphibole, clinopyroxene and plagioclase, alongside partial melting. Olivine, the most abundant xenolith mineral, is Fo_{90–91} in generation 1, decreasing to Fo₈₉ in generations 2 and 3. MnO contents show a broad range that straddles our experimental olivines (Fig. 5a). First generation orthopyroxene contains cores with 1.4 to 2.5 wt% Al₂O₃; second generation clinopyroxene has 1 to 4.5 wt% Al₂O₃. The closest match to the KLU-96–03 MSP assemblages in terms of Mg# and Al₂O₃ is at 0.8 GPa (Fig. 5c, d). Xenolith spinels have Mg# and Cr# that bracket the experimental MSPs (Fig. 5b). Bezmyianny amphiboles are aluminous pargasites similar to those in our two sub-liquidus experiments (Supplementary Table 2). Stage 3 plagioclase has a wide range of composition with a mode around An₆₀, similar to the single occurrence of plagioclase (An₅₆) in sub-liquidus run KLU10. No pressure estimate for the xenoliths is presented by Ionov et al. (2013), although estimated temperatures of 800–900 °C indicate significant sub-solidus re-equilibration. Calculated fO₂ is in the range NNO +1 to +1.8 log units (Shcherbakov et al., 2011).

Peridotite xenoliths from Kharchinsky are harzburgites, dunites and wehrlites with amphibole and chromite. A wide variety of reaction textures and secondary minerals are observed (sulfides, feldspars,

phlogopite) and there is a correspondingly wide range of mineral compositions. Gabbroic xenoliths of magmatic (cumulate) origin also occur. Mineral compositions are broadly similar in both sets of xenoliths (Fig. 5). The main differences are orthopyroxene, which is typically more magnesian with slightly higher Al_2O_3 content at Kharchinsky (Fig. 5d), and Karchinsky olivines that do not extend to low MnO at Fo_{90} (Fig. 5a). Kharchinsky amphiboles, occurring in veins and reaction relationship with clinopyroxene, are aluminous pargasites with ≤ 16 wt % Al_2O_3 and Mg# of 88 to 62. Kharchinsky xenoliths show less extensive sub-solidus re-equilibration, with estimated crystallization temperatures of up to 1140 °C; pressure is not well constrained.

Overall, good agreement in mineral chemistry between MSP experiments and peridotite xenoliths suggests that the latter are plausible representatives of the mantle source region of KLU-96-03. Some phenocryst cores may also originate by entrainment from the source region, but the bulk of the phenocrysts grew during decompression from more evolved melts.

4.2. Comparison to melt inclusions

Melt inclusion analyses from Fo_{88-90} olivine phenocrysts in Klyuchevskoy volcanics are presented by numerous authors, including Sobolev & Chaussidon (1996), Churikova et al. (2007), Portnyagin et al. (2007), Auer et al. (2009) and Mironov & Portnyagin (2011). Dissolved H_2O contents vary from < 1 to 7.1 wt%, in part due to the combined effects of H_2O increase through magmatic differentiation and diffusive H_2O -loss during cooling. Based on melt inclusion analyses, H_2O contents for Klyuchevskoy primitive melts in equilibrium with Fo_{90} are estimated to be between 3.5 and 5.3 wt%, bracketing our experimental MSPs (Table 2). This range of dissolved H_2O is shown by dashed blue lines on Fig. 5a.

For basaltic andesites ('magnesian basalts' in the terminology of Mironov and Portnyagin, 2011) similar to KLU-96-03 the best estimate of initial H_2O contents is 3.5 wt% in excellent agreement with our MSP (4.0 ± 0.5 wt%). Fluid inclusions from the same olivines record trapping pressures of 0.52 to 0.55 GPa at 1200–1250 °C (Mironov and Portnyagin, 2011). The CO_2 content of the coexisting melt was calculated to be 0.45 wt%, in good agreement with the experimental MSPs where CO_2 content is 0.42 to 0.60 wt% (Table 2). Combining the melt inclusion H_2O (3.5 wt%) and CO_2 (0.45 wt%) contents yields a calculated (MagmaSat; Ghiorso and Gualda, 2014) melt inclusion trapping pressure of 0.66 GPa in equilibrium with a fluid having molar $\text{H}_2\text{O}/(\text{H}_2\text{O}+\text{CO}_2)$ of 0.3. These conditions are entirely consistent with those derived from our MSP experiments (Table 2), suggesting that some magnesian olivine phenocrysts in basaltic andesites are derived from the magma source region or grew shortly after segregation. Mironov & Portnyagin (2011) prefer an even deeper (1.0 GPa) magmatic source with 3.5 wt% H_2O and up to 0.9 wt% CO_2 . Our experimental MSPs at 0.6 to 1.0 GPa also support a deeper mantle origin for Klyuchevskoy basaltic andesites.

4.3. Comparison with eruption temperatures

Kersting & Arculus (1994) concluded, based on mineral and whole-rock chemistry, that basalt and basaltic-andesite magmas of Kluchevskoy originated near the base of crust (0.5 – 0.9 GPa) and record high crystallisation temperatures of ≥ 1150 °C consistent with the estimates from fluid inclusion densities of Mironov and Portnyagin (2011). Eruption temperatures calculated for KLU-96-03 using olivine-melt thermometers (Putirka et al., 2008) give temperatures of 1260 – 1270 °C (Fig. 5a). The difference between crystallisation temperature estimated by Kersting & Arculus (1994) and source temperature obtained in the MSP runs is only 20–50 °C, suggesting that KLU-96-03 must have ascended slightly sub-adiabatically; adiabatic cooling for ascent of hydrous basaltic magmas is around 12 °C GPa^{-1} (Müntener et al., 2021). Phenocryst crystallisation in KLU-96-03 is most likely driven by decompression and degassing rather than by cooling.

4.4. Melt fraction calculations

To assess the degree of melting required to generate KLU-96-03 from lherzolite of the sub-arc mantle wedge we have performed mass balance calculations of MSP run products against two plausible end-member source lithologies: depleted mantle lherzolite DMM1 (Wasylenski et al., 2003) and a metaomatised, amphibole peridotite (BZ-72; Brooker et al., 2004) from ancient mantle wedge. For each mass balance calculation, we take the experimental minerals (olivine, pyroxenes, spinel) and melt from four MSP experiments (KLU11, 14, 18, 23) and regress against DMM1 and BZ-72. Ni and Cr are included in the mass balance.

Calculated melt fractions vary from 8 to 11 wt% for DMM1 (Table 3a) and 13 to 17 wt% for BZ72 (Table 3b). The best match, in terms of sum of squares of residuals is for experiment KLU11 (1220 °C, 0.7 GPa) with BZ72. In all cases the residue is a harzburgite with < 5 wt% clinopyroxene. This mineralogy is similar to peridotite xenoliths from Bezmyanny and Kharchinsky volcanoes. The degree of melting matches that invoked for Klyuchevskoy (10–13 wt%) on the basis of trace element systematics in olivine-hosted melt inclusions (Iveson et al., 2021). For a more magnesian (11.7 wt% high-MgO) primitive basalt from Klyuchevskoy, Bergal-Kuvikas et al. (2017) estimate 13.2% melting of a depleted mantle source.

Source H_2O contents, calculated using the approach of Kelley et al. (2006) with bulk solid-melt H_2O partition coefficient of 0.012, lie in the range 0.27 to 0.72 wt% (Table 3). These values overlap the source H_2O estimate (0.72 ± 0.07 wt%) of Bergal-Kuvikas et al. (2017), calculated on the basis of melt H_2O of 5.1 ± 0.5 wt%. Importantly, all of our calculated values are greater than could be stored in anhydrous mantle minerals alone (< 200 ppm for lherzolite; Kovács et al., 2012). However, an amphibole-bearing lherzolite source, such as BZ72, could contain the requisite H_2O (≥ 0.45 wt%; Green et al., 2014). Although no liquidus amphibole was found in our experiments, its occurrence at temperatures of just 20 °C below MSP (Table 2), in accordance with amphibole stability of under reduced $a\text{H}_2\text{O}$ (Juricek and Keppler, 2023), suggest that peritectic amphibole breakdown may have played an important role in melt generation. The abundance of amphibole in peridotite xenoliths from Bezmyanny and Kharchinsky supports the presence of amphibole in the source region of KLU-96-03. We conclude that KLU-96-03 originated through partial melting of a depleted amphibole-lherzolite at or slightly above the amphibole breakdown temperature at reduced $a\text{H}_2\text{O}$ (~ 0.4).

4.5. Comparison to geophysics

To compare the experimental results to geophysics requires conversion of pressures to depths. To do this we use lithostatic pressures within a crust of depth-varying density. We adopt the density model of Fedotov et al. (2010) with the following layers (depths in km relative to sea level): > 40 km, mantle peridotite, 3.25 g/cm^3 ; 40 – 30 km, mantle-crust transition zone, 3.1 g/cm^3 ; 30 – 20 km, basaltic layer, 2.9 g/cm^3 ; 20 – 6 km, granitic layer, 2.8 g/cm^3 ; 6 – 2 km, sedimentary layer, 2.6 g/cm^3 ; 2 km – surface, volcanic layer, 2.2 g/cm^3 . Taking as our datum the plain around Klyuchevskoy (1 km above sea-level), we fit this layered structure with an equation of the form (Tomiyama et al., 2010):

$$\rho(z) = \rho_1 + \alpha z - (\rho_1 - \rho_0)\exp(-z/d) \quad (1)$$

Where z is depth in km below datum and density is in g/cm^3 . Regression yields fit parameters: $\rho_1 = 2.6786$; $\rho_0 = 2.1721$; $\alpha = 0.01006$; $d = 4.4699$. Pressure (in GPa) as a function of depth (z in km) can be obtained by integration of (1):

$$P = 0.001 \times g \times \left\{ \rho_1 z + \frac{1}{2} \alpha z^2 + d(\rho_1 - \rho_0)[\exp(-z/d) - 1] \right\} \quad (2)$$

Where $g = 9.81 \text{ m}/\text{s}^2$. We do not include the effect of edifice load on lithostatic pressure, which is negligible at near-Moho depths.

Table 3

Results of mass balance calculations of melt fraction in the KLU-96–03 source region. (a) DMM1 depleted peridotite (Wasylenki et al., 2003).

| (a) DMM1 depleted peridotite (Wasylenki et al., 2003) | | | | | | | | | | |
|---|---------|--------|----------------------------------|------------|------------|------------|-----------|----|------|------------------------------------|
| run | P (GPa) | T (°C) | H ₂ O ^{melt} | melt | olivine | opx | cpx | sp | SSR | H ₂ O ^{source} |
| KLU11 | 0.7 | 1220 | 3.87 | 10.4 ± 2.4 | 72.1 ± 2.4 | 12.9 ± 4.1 | 4.9 ± 2.1 | tr | 0.43 | 0.44 |
| KLU23 | 0.6 | 1240 | 3.06 | 7.8 ± 4.4 | 71.6 ± 4.5 | 16.8 ± 7.1 | 5.0 ± 3.4 | tr | 1.43 | 0.27 |
| KLU14 | 0.8 | 1220 | 3.91 | 11.1 ± 3.6 | 75.7 ± 3.6 | 9.4 ± 5.9 | 5.1 ± 3.5 | tr | 1.21 | 0.48 |
| KLU18 | 0.6 | 1220 | 4.10 | 9.0 ± 5.0 | 72.6 ± 5.2 | 15.7 ± 8.6 | 4.3 ± 4.1 | tr | 1.82 | 0.41 |

| (b) BZ-72 amphibole peridotite (Brooker et al., 2004) | | | | | | | | | | |
|---|---------|--------|----------------------------------|------------|------------|------------|-----------|----|------|------------------------------------|
| run | P (GPa) | T (°C) | H ₂ O ^{melt} | melt | olivine | opx | cpx | sp | SSR | H ₂ O ^{source} |
| KLU11 | 0.7 | 1220 | 3.87 | 16.7 ± 1.3 | 63.8 ± 1.3 | 13.9 ± 2.1 | 4.6 ± 1.1 | tr | 0.12 | 0.68 |
| KLU23 | 0.6 | 1240 | 3.06 | 13.2 ± 3.0 | 63.1 ± 3.1 | 18.1 ± 4.8 | 5.1 ± 2.3 | tr | 0.67 | 0.44 |
| KLU14 | 0.8 | 1220 | 3.91 | 17.3 ± 2.4 | 66.9 ± 2.3 | 10.7 ± 3.9 | 4.8 ± 2.2 | tr | 0.52 | 0.72 |
| KLU18 | 0.6 | 1220 | 4.10 | 15.0 ± 3.5 | 63.9 ± 3.6 | 16.9 ± 6.1 | 4.1 ± 2.9 | tr | 0.90 | 0.66 |

Results of least squares regressions of MSP run product compositions against depleted peridotite composition DMM1.

Phase proportions and H₂O contents in wt% with 1 s.e.

tr indicates proportion within uncertainty of zero.

SSR is sum of squares of residuals.

H₂O^{source} is the H₂O content of the mantle source calculated from the melt fraction, melt H₂O content and $D(\text{H}_2\text{O}) = 0.012$ (Kelley et al., 2006).

Using Eq. (2) we calculate 0.6 GPa to be equivalent to a depth of 22.7 km below and 1.0 GPa to 36.4 km. Hypocentres of volcano-tectonic earthquakes directly beneath Klyuchevskoy cluster tightly in the range 26 to 40 km below surface (Fedotov et al., 2010; Koulakov et al., 2017) within a region of reduced P- and S-wave velocities and elevated Vp/Vs. This region is considered by Fedotov et al. (2010) as a ‘crust-mantle transition zone’ and by Koulakov et al. (2017) as the ‘top of the mantle [magma] conduit’ (Fig. 5b). This region straddles the Moho (~30 km below surface) and is considered by both groups of authors to be the source of Klyuchevskoy magmas, albeit ‘magnesian basalts’ in their terminology. Our experimental MSPs provide the additional constraint that this region comprises partially-molten peridotite. The depth of last equilibration of the basaltic andesites corresponds to the top of the seismogenic zone of Fedotov et al. (2010). Soubestre et al. (2019) identify a 20 km deep source for a volcanic tremor event in 2009 directly beneath Klyuchevskoy. This depth lies just above that derived from our MSP experiments and around the fluid inclusion trapping pressures of Mironov and Portnyagin (2011) that require the presence of a free fluid phase, capable of generating tremor. Finally, on the basis of electrical conductivity, Belyavskii (2021) proposes a melt fraction of 5–10% at 30 km depth below Klyuchevskoy.

Geophysical images of the crust beneath Klyuchevskoy identify a narrow conduit extending from the deeper seismogenic region to a shallower, more diffuse seismogenic zone at depths of 2 to 10 km below surface (Fedotov et al., 2010; Koulakov et al., 2017). Fedotov et al. (2010) suggest that this shallower region is the source of more evolved, broadly andesitic magmas, whereas Koulakov et al. (2017) suggest that this depth represents the degassing limit of ascending volatile-bearing magmas. The latter interpretation accords better with our experimental results given that multiple saturation requires dissolved H₂O contents of 3.5 ± 0.5 wt%. The calculated H₂O saturation pressures that correspond to 3 and 4 wt% H₂O at 1230 °C (using MagmaSat) are 0.09 and 0.14 GPa respectively. Higher saturation pressures would result if we account for CO₂ in the magmas, although the volume of exsolved gas increases dramatically at the point of H₂O saturation because of its much greater solubility relative to CO₂. Moreover, H₂O-saturation corresponds to the depth at which copious phenocryst crystallisation is most likely to begin due to the effect of H₂O on liquidus temperature (Blundy et al., 2010). Using Eq. (2) we translate the calculated fluid saturation pressures to depths of 3.9 to 5.9 km below surface, in excellent agreement with shallow hypocentre locations. We suggest this is a region where magmas stall, degas and crystallise during ascent albeit with little associated cooling.

5. Implications and conclusions

Our experimental results place new constraints on the thermal structure and melting conditions of mantle wedge beneath the Central Kamchatka Depression. The demonstrably primary nature of the studied basaltic andesite indicates that depleted peridotite lies at depths of 23 to 36 km below the surface, close to the sub-arc Moho. Although occurrence of peridotite at the Moho is unsurprising, the elevated temperature of melt generation at these depths (1220–1240 °C) is more than 300 °C higher than predicted by steady-state numerical models of the sub-arc geothermal gradient (e.g. Plank et al., 2009; Syracuse et al., 2010). This suggests significant ascent of hot asthenospheric mantle from deeper in the wedge, likely due to crustal extension and thinning in the CKD.

In Fig. 6 we show the location of the Klyuchevskoy basaltic andesite MSP alongside thermal models for the CKD from Syracuse et al. (2010) at two different distances from the trench (217.5 and 265.5 km). Displacement of the MSP to significantly higher temperatures than the steady-state geotherm is readily apparent. We also plot all other lherzolite MSPs listed in Table S1 for a range of subduction-related primary magma compositions ranging from MgO-rich basalt to high-magnesian andesite. Although these samples derive from a variety of arcs with different thermal structures to Kamchatka, they all testify to the presence of mantle-source peridotites at depths close to the sub-arc Moho and at temperatures well above likely steady-state geotherms. The vertical displacement is on the order 20 to 40 km with a general trend towards more mafic magmas being hotter and drier and derived from greater depths. Predictably, the driest melts (< 1 wt% H₂O) are displaced towards the anhydrous DMM1 solidus of Wasylenki et al. (2003).

Also shown on Fig. 6 are the experimental amphibole-out curves in lherzolite for different $a\text{H}_2\text{O}$ from Juricek & Keppler (2023) that emphasise the greater thermal stability for amphibole in sub-arc mantle than previously envisaged on the basis of $a\text{H}_2\text{O} \approx 1$ experiments (e.g. Green et al., 2014). The amphibole-out curves lie within ~ 25 °C of the solidus (Juricek and Keppler, 2023), thus they mark the transition from amphibole-lherzolite to lherzolite-saturated partial melt. Where these curves cross the steady-state geotherm amphibole becomes stabilised in the mantle wedge in the presence of a hydrous fluid. The depth of amphibole stabilisation varies with H₂O activity and hence fluid composition. For example, with $a\text{H}_2\text{O} = 0.25$ fluid mantle wedge at pressures below 2.4 GPa (~ 75 km) comprises amphibole peridotite; for $a\text{H}_2\text{O} = 0.5$ amphibole-peridotite occurs at pressures below 2.1 GPa (~ 65 km). At higher temperatures (and greater pressures) along the geotherm, amphibole is absent, but a low-degree hydrous partial melt is present. Thus, in subduction zones the uppermost asthenospheric

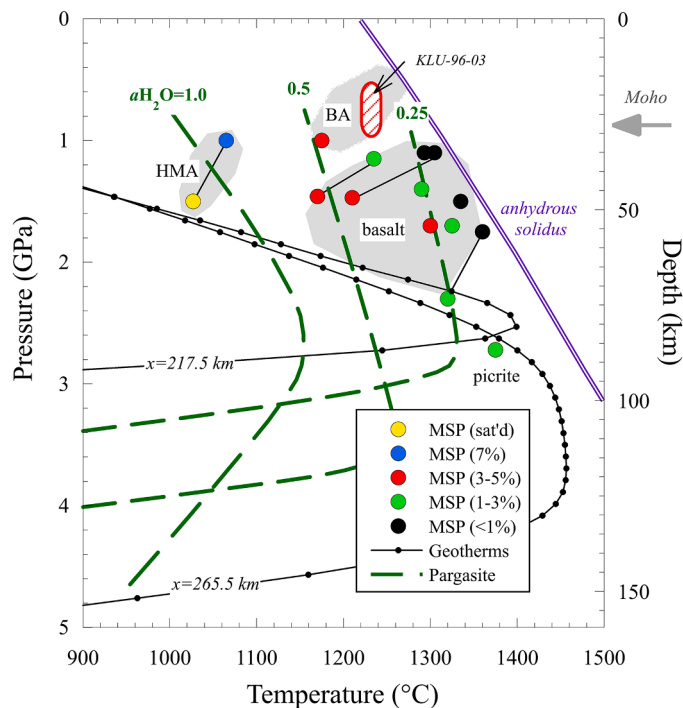


Fig. 6. Pressure-temperature plot showing experimentally-determined mantle peridotite multiple saturation points (MSP) from this study and published data (Table S1). Approximate depths on the right-hand axis are in km. Each filled circle represents a multiple saturation point in which an erupted lava was found to have the four peridotite phases olivine-orthopyroxene-clinopyroxene-spinel \pm garnet \pm phlogopite. Tie-lines connect experiments performed on the same starting material but with different H_2O . Melts are colour-coded by dissolved H_2O content (%) in legend and subdivided collectively by magma type: high-magnesian andesite (HMA), basaltic andesite (BA), basalt and picrite on the basis of major element chemistry. The pink rectangle with red outline is for basaltic andesite KLU-96-03. Oxygen fugacity (calculated from olivine-melt K_{Fe-Mg} using the method of Blundy et al. (2022) for saturation with olivine Fe_{90}) ranges from $\Delta NNO = -1.8$ to $+2.3$ log units for all experiments. MSPs map out magma source depth conditions in the sub-arc mantle wedge. Solid black lines with dots show two modelled steady-state geotherms for the Kamchatka arc from Syracuse et al. (2010) at distances of 217.5 and 265.5 km from the trench; Klyuchevskoy lies approximately 240 km from the trench (Fig. 1). The Klyuchevskoy MSP (and all other MSPs) lies well above the geotherm, indicating ascent of mantle material from depths of <60 km to the Moho (grey arrow). Green dashed lines show the upper thermal stability of amphibole at different H_2O activities (a_{H_2O}) from Juricek & Keppler (2023). Note that these curves, extrapolated below 2 GPa, match the arrays of MSPs with a consistent increase in a_{H_2O} (melt H_2O) to lower temperatures. The very low H_2O MSPs (black circles) are displaced towards the anhydrous DMM1 solidus (Wasylenski et al., 2003). Amphibole forms in mantle wedge peridotite at temperatures below the intersection of individual a_{H_2O} curves and the steady-state geotherm. Decompression of amphibole-lherzolite formed in this way gives rise to the range of observed primary arc magmas, including KLU-96-03.

mantle wedge is likely to comprise sub-solidus amphibole-lherzolite. The thickness of this amphibole-lherzolite zone depends on the thermal structure of the wedge and the composition (a_{H_2O}) of the slab-derived fluid that permeates the wedge. The amphibole-lherzolite zone is thickest for lower a_{H_2O} , cooler mantle wedge and closer to the trench. In the case of CKD, the steady-state geotherms in Fig. 6 suggests that the amphibole lherzolite zone could originally have extended to depths of 75 km. Within this depth range, mantle wedge xenoliths are expected to show a wide range of amphibole-forming metasomatic features, e.g., veining, as widely observed in Kamchatka mantle xenoliths.

H_2O remains stored in sub-solidus asthenospheric amphibole-lherzolite until pressure or temperature changes drive the lherzolite across the relevant amphibole-out curve. In the case of CKD this can be

achieved by extension of the arc, decompressing the asthenospheric mantle wedge to near-Moho depths. Decompression of amphibole-bearing lherzolite ($a_{H_2O} \approx 0.4$) lying on the geotherm at ~ 1220 °C, 2 GPa (70 km) will cross the amphibole-out curve and start to melt at ~ 1.6 GPa (50 km). Melting will continue upwards as decompression proceeds, reaching the experimentally-determined MSP at ~ 1 GPa when the basaltic andesite melt segregates from its source and ceases to be in chemical equilibrium with lherzolite. We suggest that the prominent P- and S-wave anomaly beneath the CKD that extends from the Moho to ≤ 70 km (Koulakov et al., 2020) corresponds to a region of partial melting caused by amphibole-lherzolite decompression. Thus, Klyuchevskoy basaltic andesite can be considered as products of low-degree ($\leq 10\%$) decompression melting of amphibole lherzolite in an arc-rift setting. This is in excellent agreement with Foden & Green (1992) who proposed, on the basis of phase equilibrium experiments, that arc basaltic andesites can be generated by partial melting of hornblende peridotite by wall-rock buffering along the amphibole peritectic at or close to the Moho. The value of a_{H_2O} (~ 0.4 ; Fig. 6) likely reflects the composition of the slab-derived fluids in this region.

Although our focus is on magmatism in the CKD, Fig. 6 has implications for arc magmatism in other settings. The array of MSPs for a variety of primary arc magmas closely matches amphibole-out curves at various a_{H_2O} extrapolated from Juricek & Keppler (2023) to pressures < 2 GPa with a corresponding change in magma chemistry. At $a_{H_2O} = 0.25$ melts are broadly basaltic with dissolved H_2O contents of 1 to 3 wt %; at $a_{H_2O} = 0.5$ melts are basaltic andesites with 3 to 5 wt% H_2O ; high magnesian andesite melts with ≥ 7 wt% H_2O form at lower pressures with $a_{H_2O} = 1$. In all cases the MSPs are displaced to lower pressures than would be expected from steady-state geotherms further supporting the suggestion that decompression melting of amphibole lherzolite at variable a_{H_2O} can generate a diversity of primary arc magmas.

Reduced a_{H_2O} in slab-derived fluids indicates that the fluid is not pure H_2O . This is consistent with high solute contents of slab fluids and dilution by other volatile species, including CO_2 , halogens and SO_2 . In a review of subduction zone fluids based on analyses of fluid inclusions from natural samples, Frezzotti & Ferando (2015) show that subduction zone fluids are rarely, if ever, pure H_2O ; solute contents range from < 3 to 50% $NaCl_{eq}$. Percolation of such fluids through the mantle wedge will impose $a_{H_2O} < 1$; the exact value depends on the composition and mass fraction of percolating fluids. With increasing reaction with peridotite, fluid solute loads will increase and a_{H_2O} become further reduced. We suggest that an important process in primary arc magma generation is the imposed activity of H_2O in the wedge driven by slab-fluid percolation and reaction. Stabilisation of amphibole followed by decompression-driven melting are important magma generating processes in many arcs. In some arcs, where slab-derived fluids are K-rich, such as the Colima Graben, Mexico, phlogopite mica may be main H_2O -hosting phase (Becerra-Torres et al., 2021). In both cases, decompression melting may be driven by intra-arc rifting, as in the case of CKD or Colima, or by buoyancy due to the density-reducing effect of amphibole (or phlogopite) formation.

We conclude that multiple saturation points of primary arc magmas provide an important tool for constraining the depth at which magmas segregate from their mantle sources. The tendency for these MSPs to track amphibole- (or phlogopite-) out curves for different H_2O activities supports the view that amphibole (or phlogopite) dehydration melting exercises a strong control on melt production and composition beneath arcs. In this view, mantle wedge metasomatism (to form hydrous minerals) and decompression melting, as widely invoked in models of arc magmatism (e.g. Schmidt and Jagoutz, 2017), are successive, rather than separate, magma generating processes. Previous proposals for amphibole-lherzolite dehydration melting (Davies and Stevenson, 1992) describe a similar concept but place dehydration melting reactions and magma sourcing at much greater depths (~ 80 km) than envisaged here.

CRediT authorship contribution statement

Elena Melekhova: Writing – review & editing, Writing – original draft, Methodology, Investigation, Funding acquisition, Conceptualization. **Jon Blundy:** Writing – review & editing, Writing – original draft, Methodology, Investigation, Funding acquisition, Conceptualization.

Declaration of competing interest

The authors declare that they have no known competing financial interests or personal relationships that could have appeared to influence the work reported in this paper.

Data availability

All data used in the manuscript are provided.

Acknowledgments

We are grateful to G. Wörner for providing KLU-96–03 sample which was used as starting material for our experiments. A. Matzen and K. Sokol are thanked for support on the electron microprobe and scanning electron microprobe facilities at University of Oxford. We are grateful to C.-J. de Hoog for assistance with SIMS analyses at the NERC Ion Microprobe Facility. We thank P. Van Keken for discussions about arc thermal structure and Simon Stephenson for insights into the density of Kamchatkan crust. We thank J. Badro for editorial handling and H. O'Neill for a thorough and constructive review.

Funding and Rights Retention

The work was supported by a NERC grant (NE/N001966/1) to JB and EM, and a Research Professorship from the Royal Society (RP\R1\201048) to JB. For the purpose of Open Access, the author has applied a CC BY public copyright licence to any Author Accepted Manuscript (AAM) version arising from this submission.

Supplementary materials

Supplementary material associated with this article can be found, in the online version, at [doi:10.1016/j.epsl.2024.118791](https://doi.org/10.1016/j.epsl.2024.118791).

References

- Almeev, R.R., Ariskin, A.A., Kimura, J.I., Barmina, G.S., 2013. The role of polybaric crystallization in genesis of andesitic magmas: phase equilibria simulations of the Bezmianny volcanic subseries. *J. Volcanol. Geotherm. Res.* 263, 182–192.
- Asimow, P.D., Longhi, J., 2004. The significance of multiple saturation points in the context of polybaric near-fractional melting. *J. Petrol.* 45 (12), 2349–2367.
- Auer, S., Bindeman, I., Wallace, P., Ponomareva, V., Portnyagin, M., 2009. The origin of hydrous, high- δ 18 O voluminous volcanism: diverse oxygen isotope values and high magmatic water contents within the volcanic record of Klyuchevskoy volcano, Kamchatka, Russia. *Contribut. Mineral. Petrol.* 157, 209–230.
- Baker, M.B., Grove, T.L., Price, R., 1994. Primitive basalts and andesites from the Mt. Shasta region, N. California: products of varying melt fraction and water content. *Contribut. Mineral. Petrol.* 118, 111–129.
- Ballhaus, C., Berry, R.F., Green, D.H., 1991. High pressure experimental calibration of the olivine-orthopyroxene-spinel oxygen geobarometer: implications for the oxidation state of the upper mantle. *Contribut. Mineral. Petrol.* 107, 27–40.
- Becerra-Torres, E., Melekhova, E., Blundy, J.D., Brooker, R.A., 2020. Experimental evidence for decompression melting of metasomatized mantle beneath Colima Graben, Mexico. *Contribut. Mineral. Petrol.* 175, 1–21.
- Belyavskii, V.V., 2021. Electrical conductivity and fluid distribution in the Koryak–Kamchatka region. *Izvestiya, Phys. Solid Earth* 57, 492–507.
- ... & Bergal-Kuvikas, O., Nakagawa, M., Kuritani, T., Muravyev, Y., Malik, N., Klimentko, E., Shimada, S., 2017. A petrological and geochemical study on time-series samples from Klyuchevskoy volcano, Kamchatka arc. *Contribut. Mineral. Petrol.* 172, 1–16.
- Blundy, J., Cashman, K.V., Rust, A., Witham, F., 2010. A case for CO₂-rich arc magmas. *Earth Planet. Sci. Lett.* 290 (3–4), 289–301.
- Blundy, J., 2022. Chemical differentiation by mineralogical buffering in crustal hot zones. *J. Petrol.* 63 (7), egac054.
- Bouilhol, P., Burg, J.P., Bodinier, J.L., Schmidt, M.W., Dawood, H., Hussain, S., 2009. Magma and fluid percolation in arc to forearc mantle: evidence from Sapat (Kohistan, Northern Pakistan). *Lithos* 107 (1–2), 17–37.
- Bowman, E.E., Ducea, M.N., 2023. Pyroxenite melting at subduction zones. *Geology* 51 (4), 383–386.
- Brooker, R.A., James, R.H., Blundy, J.D., 2004. Trace elements and Li isotope systematics in Zabargad peridotites: evidence of ancient subduction processes in the Red Sea mantle. *Chem. Geol.* 212 (1–2), 179–204.
- Burnham, C.W., 1979. The importance of volatile constituents. In: Yoder, H.S. (Ed.), *The Evolution of Igneous Rocks*. Princeton University Press, pp. 439–482.
- Churikova, T., Dorendorf, F., Wörner, G., 2001. Sources and fluids in the mantle wedge below Kamchatka, evidence from across-arc geochemical variation. *J. Petrol.* 42 (8), 1567–1593.
- Churikova, T., Wörner, G., Mironov, N., Kronz, A., 2007. Volatile (S, Cl and F) and fluid mobile trace element compositions in melt inclusions: implications for variable fluid sources across the Kamchatka arc. *Contribut. Mineral. Petrol.* 154, 217–239.
- Davies, J.H., Stevenson, D.J., 1992. Physical model of source region of subduction zone volcanics. *J. Geophys. Res.: Solid Earth* 97 (B2), 2037–2070.
- Davydova, M.Y., Martynov, Y.A., Perepelov, A.B., 2019. Evolution of the isotopic-geochemical composition of rocks of Uksichan Volcano, Sredinnyi Range, Kamchatka, and its relations to the tectonic restyling of Kamchatka in the Neogene. *Petrology* 27, 265–290.
- Foden, J.D., Green, D.H., 1992. Possible role of amphibole in the origin of andesite: some experimental and natural evidence. *Contribut. Mineral. Petrol.* 109 (4), 479–493.
- Frezzotti, M.L., Ferrando, S., 2015. The chemical behavior of fluids released during deep subduction based on fluid inclusions. *Am. Mineral.* 100 (2–3), 352–377.
- Gaetani, G.A., Grove, T.L., 1998. The influence of water on melting of mantle peridotite. *Contribut. Mineral. Petrol.* 131, 323–346.
- Gaetani, G.A., Grove, T.L., 2003. Experimental constraints on melt generation in the mantle wedge. Washington DC Am. Geophys. Union Geophys. Monograph Ser. 138, 107–134.
- Gualda, G.A., Ghiorsio, M.S., 2014. Phase-equilibrium geobarometers for silicic rocks based on rhyolite-MELTS. Part 1: principles, procedures, and evaluation of the method. *Contribut. Mineral. Petrol.* 168, 1–17.
- Green, D.H., Hiberson, W.O., Rosenthal, A., Kovács, I., Yaxley, G.M., Falloon, T.J., Brink, F., 2014. Experimental study of the influence of water on melting and phase assemblages in the upper mantle. *J. Petrol.* 55 (10), 2067–2096.
- Grove, T.L., Elkins-Tanton, L.T., Parman, S.W., Chatterjee, N., Müntener, O., Gaetani, G.A., 2003. Fractional crystallization and mantle-melting controls on calc-alkaline differentiation trends. *Contribut. Mineral. Petrol.* 145, 515–533.
- Hall, L.J., Brodie, J., Wood, B.J., Carroll, M.R., 2004. Iron and water losses from hydrous basalts contained in Au80Pd20 capsules at high pressure and temperature. *Mineral. Mag.* 68 (1), 75–81.
- Hirose, K., 1997. Melting experiments on lherzolite KLB-1 under hydrous conditions and generation of high-magnesian andesitic melts. *Geology* 25, 42–44.
- Ionov, D.A., Bénard, A., Plechov, P.Y., Shcherbakov, V.D., 2013. Along-arc variations in lithospheric mantle compositions in Kamchatka, Russia: first trace element data on mantle xenoliths from the Klyuchevskoy Group volcanoes. *J. Volcanol. Geotherm. Res.* 263, 122–131.
- ... & Iveson, A.A., Humphreys, M.C., Savov, I.P., De Hoog, J.C., Turner, S.J., Churikova, T.G., Cooper, G.F., 2021. Deciphering variable mantle sources and hydrous inputs to arc magmas in Kamchatka. *Earth Planet. Sci. Lett.* 562, 116848.
- Juríček, M.P., Keppler, H., 2023. Amphibole stability, water storage in the mantle, and the nature of the lithosphere-asthenosphere boundary. *Earth Planet. Sci. Lett.* 608, 118082.
- Kägi, R., Müntener, O., Ulmer, P., Ottolini, L., 2005. Piston-cylinder experiments on H₂O undersaturated Fe-bearing systems: an experimental setup approaching f O₂ conditions of natural calc-alkaline magmas. *Am. Mineralogist* 90 (4), 708–717.
- Katz, R.F., Jones, D.W.R., Rudge, J.F., Keller, T., 2022. Physics of melt extraction from the mantle: speed and style. *Annu. Rev. Earth Planet. Sci.* 50, 507–540.
- Kelemen, P.B., Hanghøj, K., Greene, A.R., 2003. One view of the geochemistry of subduction-related magmatic arcs, with an emphasis on primitive andesite and lower crust. *Treatise Geochem.* 3, 659.
- Kelley, K.A., Plank, T., Grove, T.L., Stolper, E.M., Newman, S., Hauri, E., 2006. Mantle melting as a function of water content beneath back-arc basins. *J. Geophys. Res.: Solid Earth* (B9), 111.
- Kersting, A.B., Arculus, R.J., 1995. Pb isotope composition of Klyuchevskoy volcano, Kamchatka and North Pacific sediments: implications for magma genesis and crustal recycling in the Kamchatkan arc. *Earth Planet. Sci. Lett.* 136 (3–4), 133–148.
- Khubunaya, S.A., Bogoyavlenskii, S.O., Novgorodtseva, T.Y., Okrugina, A.I., 1994. The mineralogy of the Klyuchevskoi magnesian basalts depicting the fractionation in the magma chamber. *Volcanol. Seismol.* 15, 315–338.
- ... & Koulakov, I., Abkadyrov, I., Al Arifi, N., Deev, E., Droznina, S., Gordeev, E.I., West, M., 2017. Three different types of plumbing system beneath the neighboring active volcanoes of Tolbachik, Bezmianny, and Klyuchevskoy in Kamchatka. *J. Geophys. Res.: Solid Earth* 122 (5), 3852–3874.
- ... & Koulakov, I., Shapiro, N.M., Sens-Schönfelder, C., Luehr, B.G., Gordeev, E.I., Jakovlev, A., Stupina, T., 2020. Mantle and crustal sources of magmatic activity of Klyuchevskoy and surrounding volcanoes in Kamchatka inferred from earthquake tomography. *J. Geophys. Res.: Solid Earth* 125 (10), e2020JB020097.
- Kiryukhin, A.V., Bergal-Kuvikas, O.V., Lemzikov, M.V., 2023. Magmatic activity of Klyuchevskoy volcano triggering eruptions of Bezmianny volcano based on seismological and petrological data. *J. Volcanol. Geotherm. Res.* 442, 107892.

- Kovács, I., Green, D.H., Rosenthal, A., Hermann, J., O'Neill, H.S.C., Hibberson, W.O., Udvardi, B., 2012. An experimental study of water in nominally anhydrous minerals in the upper mantle near the water-saturated solidus. *J. Petrol.* 53 (10), 2067–2093.
- Marschall, H.R., Schumacher, J.C., 2012. Arc magmas sourced from mélange diapirs in subduction zones. *Nat. Geosci.* 5 (12), 862–867.
- Melekhova, E., Blundy, J., Robertson, R., Humphreys, M.C., 2015. Experimental evidence for polybaric differentiation of primitive arc basalt beneath St. Vincent, Lesser Antilles. *J. Petrol.* 56 (1), 161–192.
- Mironov, N.L., Portnyagin, M.V., 2011. H₂O and CO₂ in parental magmas of Klyuchevskoi volcano inferred from study of melt and fluid inclusions in olivine. *Russian Geol. Geophys.* 52 (11), 1353–1367.
- Mironov, N., Portnyagin, M., Botcharnikov, R., Gurenko, A., Hoernle, K., Holtz, F., 2015. Quantification of the CO₂ budget and H₂O–CO₂ systematics in subduction-zone magmas through the experimental hydration of melt inclusions in olivine at high H₂O pressure. *Earth Planet. Sci. Lett.* 425, 1–11.
- Müntener, O., Ulmer, P., Blundy, J.D., 2021. Superhydrous arc magmas in the Alpine context. *Elements* 17 (1), 35–40.
- Ozerov, A.Y., Girina, O.A., Zharinov, N.A., Belousov, A.B., Demyanchuk, Y.V., 2020. Eruptions in the northern group of volcanoes, in Kamchatka, during the early 21st century. *J. Volcanol. Seismol.* 14, 1–17.
- Pertermann, M., Lundstrom, C.C., 2006. Phase equilibrium experiments at 0.5 GPa and 1100–1300 °C on a basaltic andesite from Arenal volcano, Costa Rica. *J. Volcanol. Geotherm. Res.* 157 (1–3), 222–235.
- Plank, T., Cooper, L.B., Manning, C.E., 2009. Emerging geothermometers for estimating slab surface temperatures. *Nat. Geosci.* 2 (9), 611–615.
- Portnyagin, M., Bindeman, I., Hoernle, K., Hauff, F., 2007. Geochemistry of primitive lavas of the Central Kamchatka Depression: magma generation at the edge of the Pacific plate. *Geophys. Monogr.-Am. Geophys.* 172, 199.
- Putirka, K.D., 2008. Thermometers and barometers for volcanic systems. *Rev. Mineral. Geochem.* 69 (1), 61–120.
- Schmidt, M.W., Jagoutz, O., 2017. The global systematics of primitive arc melts. *Geochem. Geophys. Geosyst.* 18 (8), 2817–2854.
- Sekisova, V.S., Smirnov, S.Z., Kuzmin, D.V., Shevko, A.Y., Gora, M.P., 2021. Crust–mantle xenoliths from the Kharchinsky volcano (Central Kamchatka Depression): mineralogy and petrogenesis. *Russian Geol. Geophys.* 62 (03), 339–356.
- Shcherbakov, V.D., Plechov, P.Y., Izbekov, P.E., Shipman, J.S., 2011. Plagioclase zoning as an indicator of magma processes at Bezimianny Volcano, Kamchatka. *Contribut. Mineral. Petrol.* 162, 83–99.
- Siegrist, M., Yogodzinski, G., Bizimis, M., Fournelle, J., Churikova, T., Dektor, C., Mobley, R., 2019. Fragments of metasomatized forearc: origin and implications of mafic and ultramafic xenoliths from Kharchinsky Volcano, Kamchatka. *Geochem. Geophys. Geosyst.* 20 (9), 4426–4456.
- Sisson, T.W., Grove, T.L., 1993. Temperatures and H₂O contents of low-MgO high-alumina basalts. *Contribut. Mineral. Petrol.* 113, 167–184.
- ... & Soubestre, J., Seydoux, L., Shapiro, N.M., De Rosny, J., Droznin, D.V., Droznina, S. Y., Gordeev, E.I., 2019. Depth migration of seismovolcanic tremor sources below the Klyuchevskoy volcanic group (Kamchatka) determined from a network-based analysis. *Geophys. Res. Lett.* 46 (14), 8018–8030.
- Sobolev, A.V., Chaussidon, M., 1996. H₂O concentrations in primary melts from supra-subduction zones and mid-ocean ridges: implications for H₂O storage and recycling in the mantle. *Earth Planet. Sci. Lett.* 137 (1–4), 45–55.
- Stamper, C.C., Blundy, J.D., Arculus, R.J., Melekhova, E., 2014. Petrology of plutonic xenoliths and volcanic rocks from Grenada, Lesser Antilles. *J. Petrol.* 55 (7), 1353–1387.
- Straub, S.M., Gomez-Tuena, A., Stuart, F.M., Zellmer, G.F., Espinosa-Perena, R., Cai, Y., Iizuka, Y., 2011. Formation of hybrid arc andesites beneath thick continental crust. *Earth Planet. Sci. Lett.* 303 (3–4), 337–347.
- Syracuse, E.M., van Keken, P.E., Abers, G.A., 2010. The global range of subduction zone thermal models. *Phys. Earth Planetary Interior.* 183 (1–2), 73–90.
- Till, C.B., Grove, T.L., Withers, A.C., 2012. The beginnings of hydrous mantle wedge melting. *Contribut. Mineral. Petrol.* 163, 669–688.
- Tomiya, A., Takahashi, E., Furukawa, N., Suzuki, T., 2010. Depth and evolution of a silicic magma chamber: melting experiments on a low-K rhyolite from Usu volcano, Japan. *J. Petrol.* 51 (6), 1333–1354.
- Ubide, T., Mollo, S., Zhao, J.X., Nazzari, M., Scarlato, P., 2019. Sector-zoned clinopyroxene as a recorder of magma history, eruption triggers, and ascent rates. *Geochim. Cosmochim. Acta* 251, 265–283.
- Wasylenki, L.E., Baker, M.B., Kent, A.J., Stolper, E.M., 2003. Near-solidus melting of the shallow upper mantle: partial melting experiments on depleted peridotite. *J. Petrol.* 44 (7), 1163–1191.
- Weaver, S.L., Wallace, P.J., Johnston, A.D., 2011. A comparative study of continental vs. intraoceanic arc mantle melting: Experimentally determined phase relations of hydrous primitive melts. *Earth Planet. Sci. Lett.* 308 (1–2), 97–106.

Further Reading

- Fedotov, S.A., Zharinov, N.A., 2007. On the eruptions, deformation, and seismicity of Klyuchevskoy Volcano, Kamchatka in 1986–2005 and the mechanisms of its activity. *J. Volcanol. Seismol.* 1 (2), 71–97.
- Shishkina, T.A., Botcharnikov, R.E., Holtz, F., Almeev, R.R., Jazwa, A.M., Jakubiak, A.A., 2014. Compositional and pressure effects on the solubility of H₂O and CO₂ in mafic melts. *Chem. Geol.* 388, 112–129.